JACS
JOURNAL OF THE AMERICAN CHEMICAL SOCIETY
Cite This: J. Am. Chem. Soc. 2018, 140, 34−37
Communication
pubs.acs.org/JACS

Tilted, Uninterrupted, Monomeric HIV-1 gp41 Transmembrane Helix from Residual Dipolar Couplings

Sai Chaitanya Chiliveri,[†] John M. Louis,[†] Rodolfo Ghirlando,[‡] James L. Baber,[†] and Ad Bax*[,†]

[†]Laboratory of Chemical Physics and [‡]Laboratory of Molecular Biology, National Institute of Diabetes and Digestive and Kidney Diseases, National Institutes of Health, Bethesda, Maryland 20892, United States

Supporting Information

ABSTRACT: Cryo-electron microscopy and X-ray crystallography have shown that the pre- and postfusion states of the HIV-1 gp41 viral coat protein, although very different from one another, each adopt C_3 symmetric structures. A stable homotrimeric structure for the transmembrane domain (TM) also was modeled and supported by experimental data. For a C_3 symmetric structure, alignment in an anisotropic medium must be axially symmetric, with the unique axis of the alignment tensor coinciding with the C_3 axis. However, NMR residual dipolar couplings (RDCs) measured under three different alignment conditions were found to be incompatible with C_3 symmetry. Subsequent measurements by paramagnetic relaxation enhancement, analytical ultracentrifugation, and DEER EPR, indicate that the transmembrane domain is monomeric. ^{15}N NMR relaxation data and RDCs show that TM is highly ordered and uninterrupted for a total length of 32 residues, extending well into the membrane proximal external region.

Fusion of the human immunodeficiency virus (HIV) and host cell membranes is mediated by the viral envelope protein, Env, consisting of two polypeptide chains, gp120 and gp41. Env is similar in architecture to a wide range of other viral fusion proteins.[1] Env exists as a homotrimer of heterodimers and forms a spike on the viral surface.[2−5] Soon after binding to CD4, located on the surface of host T cells, gp120 dissociates from gp41, resulting in a cascade of conformational changes in gp41 that lead to membrane fusion.[6,7] Even though a large amount of structural information is available on the gp41 ectodomain (including the fusion peptide (FP), fusion peptide proximal region (FPPR), N-heptad repeat (NHR), immunodominant linker (IL) and C-heptad repeat (CHR)),[2−5] a comprehensive structural understanding of the membrane proximal external region (MPER), the transmembrane region (TM) and the intraviral C-terminal domain (CT) has remained elusive (Figure 1A). It is widely believed that TM adopts a trimeric helical bundle arrangement in the membrane bilayer.[7,8] However, a recent cryo-EM study of Env, lacking CT but including MPER and TM, did not show electron density for TM,[5] and analytical centrifugation studies of a construct containing MPER and TM (residues 666−715) at pH 7 in dodecylphosphocholine (DPC) micelles showed the peptide to be monomeric.[9] On the other hand, weak

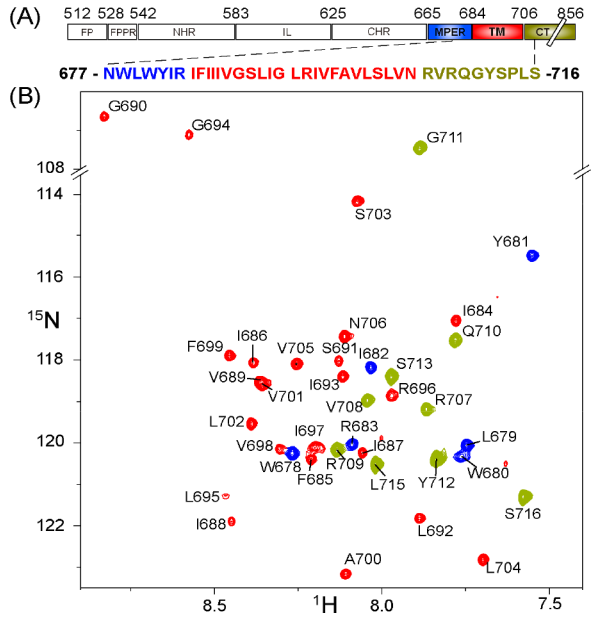

Figure 1. NMR study of HIV-1 clade D gp41-TM. (A) Domain architecture of gp41. The peptide sequence used in this study comprises residues N677 to S716. (B) Assigned ^{1}H-^{15}N TROSY-HSQC spectrum of TM in the presence of 150 mM DMPC/DHPC (q = 0.4) bicelles. Resonances from MPER, TM and CT region are color coded in blue, red and olive, respectively.

trimerization propensity was demonstrated for the TM of the analogous paramyxovirus fusion protein.[10] Recently, a structural model for isotopically labeled gp41-TM in small bicelles has been reported, based on NMR data.[11] The expected C_3-symmetric structure was of moderate resolution, owing to the relatively small number of long-range NOE restraints that could be obtained for this system.

To gain additional insights into the intermolecular interactions that could stabilize trimer formation, we set out to measure residual dipolar couplings (RDCs), which are highly precise experimental parameters reporting on bond vector orientation relative to the global principal axis system of the alignment tensor.[12−14] For a system of C_3 or higher symmetry, the alignment tensor is axially symmetric, with its unique axis parallel to the C_3 axis.[15] Although this axial symmetry has the advantage of minimizing the degrees of

Received: September 25, 2017
Published: December 26, 2017

DOI: 10.1021/jacs.7b10245
J. Am. Chem. Soc. 2018, 140, 34−37

freedom when interpreting RDCs in terms of angular orientation, tensors obtained under different alignment conditions will be linearly related by a simple scaling factor and therefore do not offer independent information. However, when we measured TM RDCs under different alignment conditions, including strained neutral and positively charged acrylamide gels,[16,17] as well as paramagnetic alignment,[18−20] the couplings were not related by simple scale factors, a finding inconsistent with C_3 symmetry. We therefore revisited the question regarding the oligomeric state of TM and, as reported below, find it to be monomeric.

A 40-residue segment (N677−S716) of HIV-1 Clade D gp41, which included the TM region, was expressed as a GB1-TM fusion construct linked by an Asp−Pro dipeptide, which was subsequently cleaved by acid hydrolysis and purified by HPLC (Supporting Information, Figure S1). With the exception of an additional Pro−Gly dipeptide at the N-terminus, this sequence is identical to that used by Dev et al.[11] Use of the same mixed micelle (small bicelle)[21] system as used in the prior study, 1,2-dimyristoyl-*sn*-glycero-3-phosphocholine (DMPC) and 1,2-dihexanoyl-*sn*-glycero-3-phosphocholine (DHPC) in a 1:2.5 molar ratio (q = 0.4), yielded a ^{1}H-^{15}N TROSY-HSQC spectrum very similar to that reported previously,[11] indicating our peptide adopts the same structure.

Secondary $^{13}C^{\alpha}$ chemical shifts confirm that residues 678 to 709 adopt a continuous α-helical conformation (Figure S3A). Residues 678 to 683, belonging to MPER, form an uninterrupted N-terminal helical extension of TM, whereas CT residues 710−716 exhibit close to random coil values.

In order to evaluate whether the peptide is well ordered, we probed its backbone dynamics by ^{15}N NMR relaxation measurements. As can be seen (Figure 2), the helical segment of the structure is remarkably homogeneous in its dynamic behavior and spans a range of over 30 residues.

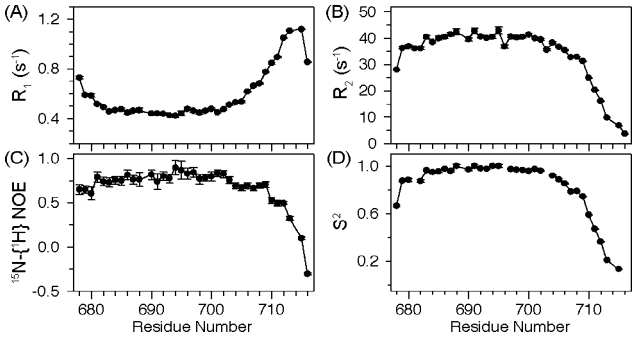

Figure 2. Backbone dynamics of gp41 TM from ^{15}N relaxation rates, measured at 900 MHz ^{1}H frequency. (A) R_1, (B) R_2 and (C) ^{15}N-{^{1}H} NOE values were subjected to standard Lipari-Szabo analysis[22,23] to yield the generalized order parameters, S^2 (D).

With generalized order parameters, $S^2 \geq 0.75$, residues I684−N706, commonly assigned to TM, are found to be as well ordered as residues typically seen in folded globular proteins. An increase in R_1 rates for N706−R709, which also adopt α-helical structure based on secondary $^{13}C^{\alpha}$ chemical shifts, points to some fraying for this last turn of helix, but NOE values ≥0.6 indicate that they should be amenable to RDC analysis. Remarkably, MPER residues L679−R683 are also well ordered, exhibiting dynamic characteristics very similar to those of TM. With an effective correlation time of ca. 21 ns, derived from R_2/R_1 ratios for the most highly ordered segment of the helix (F685−L702), the molecular tumbling time is roughly consistent with that of a 50 kDa particle. This value is close to that expected for a transmembrane helix embedded in a bicelle with q = 0.4, whose volume is dominated by the phospholipids.[21,24] Residues Q710−S716 exhibit near random coil chemical shifts and strongly elevated internal dynamics, essentially behaving as a disordered tail.

For high precision RDC measurements, we initially resorted to stretched acrylamide gels, either neutral or with a small amount of positive doping (see SI). The resulting RDCs closely correlate with one another (Figure 3; R^2 = 0.95), but

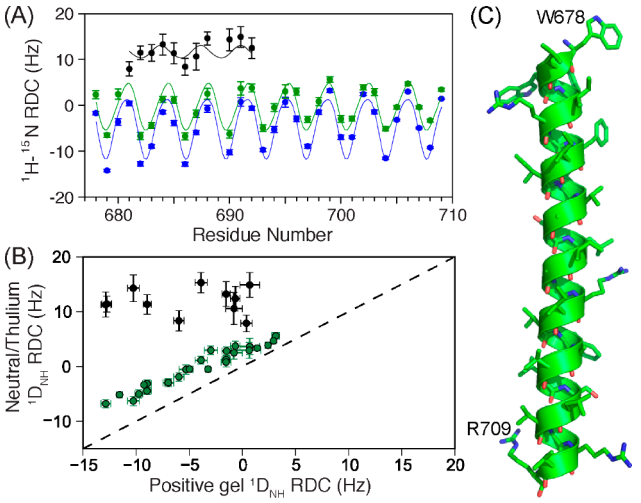

Figure 3. RDC analysis of gp41-TM. (A) ^{1}H-^{15}N residual dipolar couplings obtained by aligning TM with DOTA M8-thulium (black), stretched neutral (green) and positively charged (blue) polyacrylamide gel. Superimposed are the "dipolar wave" oscillations, calculated for an idealized perfectly straight helix, using parameters δ = 15.8° and $\rho = 2\pi n/3.6$.[25] Near axial symmetry of the thulium alignment tensor, with its unique axis within 10° of the helix axis, cause $\sin(\theta)$ oscillations to be small in amplitude.[25] (B) Correlation plot between $^1D_{NH}$ RDCs collected in neutral gel (green) or by thulium alignment (black) against values measured in positively charged gel. (C) Ribbon diagram for the ordered region of the TM helix, derived from the RDCs (PDB entry 6B3U; Figure S4).

surprisingly and in contrast to what is expected for an axially symmetric alignment tensor, the two sets of RDCs are not simply related by a scaling factor, contradicting C_3 symmetry. Nevertheless, both sets of RDCs clearly show the periodicity of 3.6 residues, indicative of a highly regular helical structure, with the time-averaged helical axis orientation tilted at angles of *ca* 60° and 70° relative to the magnetic field in neutral and positively charged gels, respectively.[25]

With the range of different alignments achievable in gel compositions remaining rather limited (Table S3), we also resorted to paramagnetic alignment by attachment of a 4R,4S-DOTA-M8 tag[20] at position 707, using a R707C mutant of the TM peptide. The difference between $^1J_{NH}$ splitting with the tag chelated to paramagnetic thulium and diamagnetic lutetium corresponds to the RDC. Outside the S703−G711 region, resonance positions for the diamagnetic form were essentially indistinguishable from those in Figure 1, indicating that the R707C mutation caused no significant structural perturbation. For the thulium tagged molecule, proximate residues R696−Q710 were severely broadened by paramagnetic relaxation, prohibiting RDC measurement. However, RDCs were

DOI: 10.1021/jacs.7b10245
J. Am. Chem. Soc. 2018, 140, 34−37

measurable at a reasonable level of precision for the more remote N-terminal segment, yielding relatively uniform positive values of ca. 12 Hz ($^1J_{NH}$ splitting of ca. 80 Hz), corresponding to the time-averaged helix axis orientation approximately collinear with the magnetic field. The finding of different RDCs for the three alignment mechanisms, not related by a simple scale factor, is fundamentally incompatible with a C_3 symmetric structure. We therefore calculated the structure without symmetry restrictions, using standard protocols and both using a floating set of alignment tensors, as well as a systematic grid search varying alignment strength (D_a) and rhombicity (Rh) independently, yielding indistinguishable results. Restraining the backbone torsion angles of residues 678−709 to α-helical values by means of a harmonic potential that includes a broad (40° width) flat bottom, as well as a hydrogen bond database potential,[26] improved convergence of the RDC-based structure calculations and yielded models with excellent cross validation statistics (Q_{free} 15−20%; SI Table S2). Note that when deriving Q_{free},[27−29] we simultaneously left out all three RDCs measured for a given amide, and repeated the structure calculation 31 times, each time omitting data for a different residue. Structures for the region 679−709 adopt near perfect helical dihedral angles with average ϕ and ψ values of −61.6° and −43.3°, respectively (Figure S4). The structures show an extended nearly 9-turn α-helix formed by residues 678−709 (Figure 3C and S4). Remarkably, there is no disruption in helical structure between TM and MPER residues (L679−R683). Interestingly, the presumed TM segment (I684−N706) also extends for a full turn in the C-terminal direction (R707−R709), even though ^{15}N relaxation data point to a modest drop in order parameter for this last turn of helix (Figure 2D). With a length of ∼45 Å, the 32-residue helix is considerably longer than most transmembrane helices, suggesting it cannot be parallel to the bilayer normal.

To further investigate the oligomerization state of TM, paramagnetic relaxation enhancement (PRE) measurements were carried out, attaching a nitroxyl spin radical, MTSL, to C707 of the R707C mutant. ^{1}H-R_2 rates were measured under both paramagnetic and diamagnetic conditions on a sample containing one equivalent of ^{15}N TM (native sequence) and two molar equivalents of ^{14}N TM R707C-MTSL (Figure 4A). For a parallel oligomeric arrangement of TM helices, a pronounced increase in R_2 rates of the C-terminal residues of the ^{15}N TM would be expected. However, besides the nearly uniform small increase across all amide protons, no evidence for intermolecular PRE is observed, indicating TM is monomeric under the conditions of our study.

Density matched (92.5% D_2O; Figure S5B) sedimentation equilibrium (SE) analytical ultracentrifugation was then performed to further evaluate the oligomerization state of TM.[10] As the density of bicelles is higher than that of the solvent buffer, density matching with D_2O was performed to nullify the sedimentation effect of bicelles. Because the mass of the peptide is much smaller than that of the bicelle, resulting in only a very small fractional change in mass between different peptide oligomerization states, we carried out the measurements on the uncleaved GB1-TM construct (14.9 kDa). The GB1 tag did not induce any structural changes in TM, as judged by the absence of peak position changes in the TROSY-HSQC spectrum (Figure S5A). Fitting the data for three speeds (10 000, 20 000 and 35 000 rpm) to a single species yielded a molecular weight of 16.5 kDa, confirming a

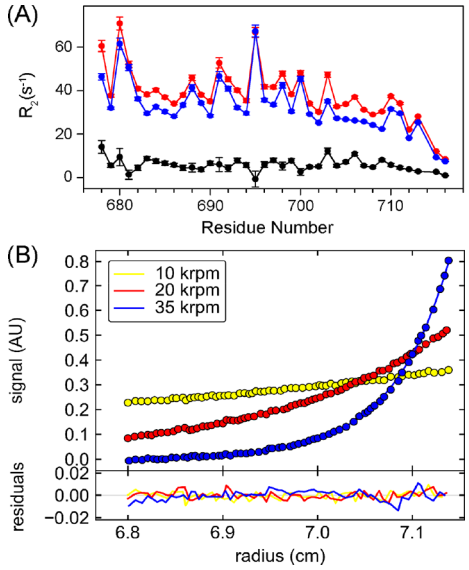

Figure 4. Evaluation of the oligomerization state of HIV-1 clade D TM. (A) $^1H^N\{-^{15}N\}$ R_2 rates in U-^{15}N, ^{2}H gp41-TM in the presence of 2 mol equiv of paramagnetic ^{14}N TM R707C-MTSL (red) and reduced nitroxide (blue) spin label. The difference in ^{1}H R_2 rates induced by the paramagnetic spin label is shown in black. Rates are listed in Table S7. (B) Sedimentation equilibrium data on the GB1-TM fusion construct (see SI). Absorbance is shown as a function of radial position at three different rotor speeds, 10 000 (yellow), 20 000 (red) and 35 000 rpm (blue). Residuals are shown in the bottom panel.

monomeric state (Figure 4B). Additionally, SE analysis of TM derived from HIV-1 clade C, indicates that the monomeric state of the TM in bicelles is not specific to clade D (Figure S5C,D).

To further investigate the TM oligomerization state, we also collected DEER EPR data over a wide range of peptide:lipid stoichiometries. In such measurements, modulation depths of ca. 0.43 and 0.68 are expected for dimers and trimers, respectively, and observed on our Q-band EPR spectrometer for other systems.[30] However, very small modulation depths in the DEER time domain data of the TM at low peptide:lipid ratios ($\leq 10^{-3}$) are only consistent with a monomeric state of TM (Figure S6). A slight increase of the small modulation depth at higher peptide:lipid stoichiometry is consistent with the statistically expected increase in the fraction of bicelles that contain more than one gp41-TM.

Our studies show that HIV-1 gp41-TM adopts a nearly straight α-helical structure when solubilized in DMPC/DHPC bicelles. The observation that RDCs in different alignment media are not related by a simple scaling factor rules out the C_3-symmetric arrangement often assumed to apply to this widely occurring structural element. Paramagnetic relaxation, analytical ultracentrifuge and pulsed EPR experiments confirm the monomeric state of the isolated TM in the bicelle model system, despite the TM:lipid ratio in our study being about 1 order of magnitude higher than in the intact virus. This result suggests that trimerization of gp41 is likely dominated by either its ecto- and/or C-terminal domain. The large length of the uninterrupted α-helix relative to the thickness of the hydrophobic interior of the lipid bilayer creates a large hydrophobic mismatch if oriented parallel to the membrane normal. Park and Opella evaluated the effect of hydrophobic mismatch for the HIV-1 Vpu 18-residue transmembrane helix

DOI: 10.1021/jacs.7b10245
J. Am. Chem. Soc. 2018, 140, 34−37

on its tilt angle, θ, as a function of bilayer thickness.[31] Their empirical equation suggests a very large tilt angle of ca. 50° for gp41-TM in a 1,2-di-O-octadecenyl-*sn*-glycero-3-phosphocholine bilayer, used by them as a mimic for the viral membrane. This angle decreases with increasing bilayer thickness, but a very large increase, or kinking of the TM, is required to allow extensive interhelical contacts in a C_3-symmetric homotrimeric arrangement.

Some helical kinks previously found in the NOE-derived trimeric structure by Dev et al.[11] are largely absent in our RDC structure, resulting in a substantial backbone coordinate RMSD relative to this earlier structure (3.6 Å; Figure S8). As commonly seen for NOE-derived structures, agreement with RDCs for a monomeric subunit ($Q = 0.57$) is modest, but RDCs are fully inconsistent with the trimeric structure (Figure S8). Our independent resonance assignments (Figure 1) fully agree with those of the prior study, indicating the state of the peptides studied is very similar. Dev's conclusion of a trimer was based, in part, on gel electrophoresis data, which are known to yield anomalous migration for helical TM peptides (see SI), but also on the observation of weak intermolecular NOE contacts in mixed label samples. If indeed intermolecular, a small fraction of dimeric or higher order oligomers in rapid exchange with a dominant monomer population could potentially reconcile our divergent conclusions.

The side chain of R683 is on the opposite helical face compared to R696 and R707, and considering the large tilt angle mentioned above, we speculate that the hydrophilic termini of these long side chains can "snorkel" to the polar regions of the opposite leaflets of the lipid bilayer. These Arg residues prevent rotation of the helix around its axis in the lipid bilayer. Together with the large helix tilt angle these residues destabilize the membrane and prime it for fusion.

■ ASSOCIATED CONTENT

Supporting Information

The Supporting Information is available free of charge on the ACS Publications website at DOI: 10.1021/jacs.7b10245.

Experimental procedures and supporting figures with additional data (PDF)

■ AUTHOR INFORMATION

Corresponding Author

*bax@nih.gov

ORCID

Ad Bax: 0000-0002-9809-5700

Notes

The authors declare no competing financial interest.

■ ACKNOWLEDGMENTS

We thank J. Ying and A. Aniana for technical support, Daniel Häussinger for providing DOTA-M8 thulium and lutetium tags, James Chou and Qingshan Fu for discussions regarding TM purification and John Lloyd for mass spectrometry. This work was supported by the Intramural Research Program of the NIDDK and by the Intramural Antiviral Target Program of the Office of the Director, NIH.

■ REFERENCES

(1) Harrison, S. C. *Nat. Struct. Mol. Biol.* **2008**, *15*, 690−698.
(2) Zhu, P.; Liu, J.; Bess, J.; Chertova, E.; Lifson, J. D.; Grise, H.; Ofek, G. A.; Taylor, K. A.; Roux, K. H. *Nature* **2006**, *441*, 847−852.
(3) Bartesaghi, A.; Merk, A.; Borgnia, M. J.; Milne, J. L. S.; Subramaniam, S. *Nat. Struct. Mol. Biol.* **2013**, *20*, 1352−1357.
(4) Lyumkis, D.; Julien, J. P.; de Val, N.; Cupo, A.; Potter, C. S.; Klasse, P. J.; Burton, D. R.; Sanders, R. W.; Moore, J. P.; Carragher, B.; Wilson, I. A.; Ward, A. B. *Science* **2013**, *342*, 1484−1490.
(5) Lee, J. H.; Ozorowski, G.; Ward, A. B. *Science* **2016**, *351*, 1043−1048.
(6) Furuta, R. A.; Wild, C. T.; Weng, Y. K.; Weiss, C. D. *Nat. Struct. Biol.* **1998**, *5*, 276−279.
(7) Blumenthal, R.; Durell, S.; Viard, M. *J. Biol. Chem.* **2012**, *287*, 40841−40849.
(8) Reichart, T. M.; Baksh, M. M.; Rhee, J. K.; Fiedler, J. D.; Sligar, S. G.; Finn, M. G.; Zwick, M. B.; Dawson, P. E. *Angew. Chem., Int. Ed.* **2016**, *55*, 2688−2692.
(9) Dai, Z.; Tao, Y. S.; Liu, N. N.; Brenowitz, M. D.; Girvin, M. E.; Lai, J. R. *Biochemistry* **2015**, *54*, 1589−1599.
(10) Smith, E. C.; Smith, S. E.; Carter, J. R.; Webb, S. R.; Gibson, K. M.; Hellman, L. M.; Fried, M. G.; Dutch, R. E. *J. Biol. Chem.* **2013**, *288*, 35726−35735.
(11) Dev, J.; Park, D.; Fu, Q. S.; Chen, J.; Ha, H. J.; Ghantous, F.; Herrmann, T.; Chang, W. T.; Liu, Z. J.; Frey, G.; Seaman, M. S.; Chen, B.; Chou, J. J. *Science* **2016**, *353*, 172−175.
(12) Tjandra, N.; Bax, A. *Science* **1997**, *278*, 1111−1114.
(13) Prestegard, J. H.; Al-Hashimi, H. M.; Tolman, J. R. *Q. Rev. Biophys.* **2000**, *33*, 371−424.
(14) Blackledge, M. *Prog. Nucl. Magn. Reson. Spectrosc.* **2005**, *46*, 23−61.
(15) Al-Hashimi, H. M.; Bolon, P. J.; Prestegard, J. H. *J. Magn. Reson.* **2000**, *142*, 153−158.
(16) Tycko, R.; Blanco, F. J.; Ishii, Y. *J. Am. Chem. Soc.* **2000**, *122*, 9340−9341.
(17) Meier, S.; Haussinger, D.; Grzesiek, S. *J. Biomol. NMR* **2002**, *24*, 351−356.
(18) Bertini, I.; Luchinat, C.; Parigi, G. *Prog. Nucl. Magn. Reson. Spectrosc.* **2002**, *40*, 249−273.
(19) Rodriguez-Castaneda, F.; Haberz, P.; Leonov, A.; Griesinger, C. *Magn. Reson. Chem.* **2006**, *44*, S10−S16.
(20) Haussinger, D.; Huang, J. R.; Grzesiek, S. *J. Am. Chem. Soc.* **2009**, *131*, 14761−14767.
(21) Vold, R. R.; Prosser, R. S.; Deese, A. J. *J. Biomol. NMR* **1997**, *9*, 329−335.
(22) Lipari, G.; Szabo, A. *J. Am. Chem. Soc.* **1982**, *104*, 4546−4559.
(23) Mandel, A. M.; Akke, M.; Palmer, A. G., III *J. Mol. Biol.* **1995**, *246*, 144−163.
(24) Lorieau, J. L.; Louis, J. M.; Bax, A. *J. Am. Chem. Soc.* **2011**, *133*, 14184−14187.
(25) Mesleh, M. F.; Opella, S. J. *J. Magn. Reson.* **2003**, *163*, 288−299.
(26) Grishaev, A.; Bax, A. *J. Am. Chem. Soc.* **2004**, *126*, 7281−7292.
(27) Cornilescu, G.; Marquardt, J. L.; Ottiger, M.; Bax, A. *J. Am. Chem. Soc.* **1998**, *120*, 6836−6837.
(28) Clore, G. M.; Garrett, D. S. *J. Am. Chem. Soc.* **1999**, *121*, 9008−9012.
(29) Bax, A. *Protein Sci.* **2003**, *12*, 1−16.
(30) Louis, J. M.; Baber, J. L.; Ghirlando, R.; Aniana, A.; Bax, A.; Roche, J. *PLoS One* **2016**, *11*, e0160597.
(31) Park, S. H.; Opella, S. J. *J. Mol. Biol.* **2005**, *350*, 310−318.

DOI: 10.1021/jacs.7b10245
J. Am. Chem. Soc. 2018, 140, 34−37